IEEE Access
Multidisciplinary | Rapid Review | Open Access Journal

Received 4 February 2025, accepted 7 March 2025, date of publication 17 March 2025, date of current version 28 March 2025.

Digital Object Identifier 10.1109/ACCESS.2025.3552186

RESEARCH ARTICLE

Blind Carrier and Noise Power and Roll-Off Factor Estimation for PCMA Signals

ANDREAS FEDER[1], (Graduate Student Member, IEEE), ADELA VAGOLLARI[1], (Graduate Student Member, IEEE), RODRIGO FISCHER[1,2], (Graduate Student Member, IEEE), MARTIN HIRSCHBECK[3], AND WOLFGANG GERSTACKER[1], (Senior Member, IEEE)

[1]Institute for Digital Communications, Friedrich–Alexander-Universität Erlangen–Nürnberg, 91058 Erlangen, Germany
[2]Communications Engineering Lab (CEL), Karlsruhe Institute of Technology, 76131 Karlsruhe, Germany
[3]Innovationszentrum für Telekommunikationstechnik GmbH IZT, 91058 Erlangen, Germany

Corresponding author: Andreas Feder (andreas.feder@fau.de)

This work was supported by the Bayerische Forschungsstiftung under Grant AZ-1544-22. The work of Adela Vagollari was supported by Bavarian Equal Opportunities Sponsorship—Realisierung von Chancengleichheit von Frauen in Forschung und Lehre (FFL).

ABSTRACT The *Paired Carrier Multiple Access* (PCMA) technology is adopted in modern satellite communication systems. It establishes duplex links between two ground stations while enhancing the bandwidth efficiency by assigning two single-carrier (SC) signals to the same time-frequency resource. For a blind receiver for the satellite downlink signal in such system, in contrast to the cooperating transceivers of the duplex link, no information about signaling, training sequences or data is available. Yet, it requires accurate knowledge about the signal and channel parameters because the task of jointly demodulating and detecting the data of both included SC signals is rather challenging. In this paper, we present several statistics based estimators for the respective powers of the SC signals and the noise from the mixture signal. We illustrate the benefits of the respective power estimation approaches for different modulation schemes by providing a performance evaluation based on numerical simulations. To provide the estimators with the knowledge of the respective roll-off factors that are used by the transmitters to generate the SC signals, we introduce a neural network classifier for roll-off factor estimation.

INDEX TERMS Blind receiver, carrier power estimation, paired carrier multiple access (PCMA), roll-off factor estimation.

I. INTRODUCTION

A duplex link between two ground stations (GSs) on earth may be established by a satellite that acts as a relay. Classically, the satellite relay allocates the two uplink signals to two distinct time-frequency resources, e.g., two separate frequency bands, in the downlink. In order to use the available bandwidth resources in the downlink more efficiently, in a *Paired Carrier Multiple Access* (PCMA) system, the satellite relay amplifies and adds up the transmit signals of the GSs, and allocates the sum to a single time-frequency resource [1]. Thereby, the required bandwidth resources in the downlink are reduced down to 50%. Such approach of an operational spectrum sharing mode has been implemented by different satellite modem manufacturers, and referred to as *Carrier-in-Carrier* or *Doubletalk* by the respective parties [2], [3].

The receivers at the respective GSs are fed not only with the received aggregate signal from the satellite downlink but also with the uplink transmit signal of this respective GS. Using the known transmit signal, its contribution to the received downlink signal is detected after passing through the uplink channel, processing at the satellite and downlink transmission, and subtracted from the sum signal. Ideally, only the part that corresponds to the transmit signal of the far-end GS impaired by additive noise remains as input to the demodulation process.

A. BLIND PCMA RECEIVER

Obviously, the improved utilization of the available frequency bands is achieved by the cooperation of the satellite relay and the two GSs at which the self-interference is known. The

The associate editor coordinating the review of this manuscript and approving it for publication was Xueqin Jiang.

focus of this paper is a further GS on earth, that does not participate in the aforementioned cooperation. Thus, it is only receiving the satellite's downlink sum signal and has no information on any of the transmit signals. No access to any signaling information or training sequences which may be embedded into the respective signal stream is assumed. Furthermore, we assume that this receiver does not possess any knowledge about the transmit signal parameters which have been determined during the setup of the communication link between the two GSs. We refer to such a GS as *blind* receiver. Applications where such a blind receiver is employed include spectral monitoring and signal interception. In compliance with such application scenarios, we assume that the blind receiver is capable to detect and localize a PCMA signal of interest within the observable frequency spectrum. Moreover, it is assumed that coarse estimates of the downlink signal bandwidth and its center frequency can be obtained. Hence, distortion-free bandpass filtering of the PCMA downlink signal that removes any adjacent channel interference is presupposed for the considerations here.

The natural aim of the blind receiver is to demodulate the data that is transmitted by the two first GSs and their single-carrier (SC) signals. For the case of similar power levels of the SC signals, the application of successive interference cancellation is not promising, and joint detection needs to be carried out instead. Multi-user sequence estimation algorithms can be employed if explicit knowledge of the channel state information and transmit signal parameters is available. In the blind receiver, estimates of these parameters need to be obtained by non-data-aided procedures and provided to the subsequent detection unit. However, also schemes that perform the detection jointly with estimation and tracking of the required parameters need to be initialized with parameter estimates of sufficient accuracy.

In the case of frequency selective channels, e.g. induced by significant multipath propagation, the sole estimation of the roll-off factors as covered in this paper does not apply and estimation of the entire channel impulse response is necessary. Here, we assume a frequency non-selective channel which is typical for a satellite downlink. It is determined mainly by the synchronization parameters as well as the carrier and noise power levels. Their values are assumed to be only slowly time-varying and hence, for the time windows used for processing steps of the parameter estimation at the receiver, are modeled as constant. This assumption may become invalid if e.g. significant oscillator drifts related to the transmitter and receiver hardware need to be regarded or the satellite movement induces Doppler shifts that result in quick variations of the frequency and phase quantities. Yet, if the assumption is met, e.g. by choosing the length of the processed time segment appropriately short, feedforward parameter estimators are realizable. The symbol rate as well as the modulation constellation and transmit pulse shape are further relevant signal parameters of the assumed linear digitally modulated transmit signals, and need to be inferred from the downlink signal at the blind receiver. The transmit pulse is assumed to be of root-raised-cosine (RRC) type with its bandwidth excess being parameterized by a roll-off factor.

B. SCOPE OF THIS PAPER

In this paper, we focus on the estimation of the powers of the two SC signals corresponding to the respective transmit signals contained in the received PCMA downlink signal, as well as the noise power. In contrast to the assumptions in [4], where identical RRC transmit pulse shapes and roll-off factors for both carrier signals are assumed, here, the respective roll-off factors of the RRC pulses of the carrier signals are modeled as in general different. Because, in this case, the knowledge of the roll-off factors facilitates the estimation of the carrier powers, we further introduce an approach for roll-off factor estimation as an enabling step.

Obviously, the signal model employed by sequence estimation schemes will be erroneous and may lead to wrongly detected symbols and sequences if the powers of the two individual SC signals within the received PCMA signal do not match the respective true values. The additional knowledge of the noise power or, equivalently, the signal-to-noise ratio (SNR), is not only beneficial for controlling the processing settings of the receiver, which may in practice be adjusted to implement certain degrees of performance or complexity. Its knowledge is also essential for detection schemes that compute a-posteriori probabilities or equivalent quantities as inputs for subsequent soft-input channel decoders [5]. As for the carrier powers, the knowledge of the roll-off factors, and thus the transmit pulse shapes, is essential for providing an accurate model of the noise-free receive signal hypotheses. Obviously, the detection process of the blind receiver operates in a regime of strong cochannel interference. Hence, avoiding any additional distortions due to inaccurate description of the contributions of the signal hypotheses to the received signal is vital for enabling joint detection of the symbol sequences of both carriers with tolerably low error rates. Furthermore, a precise knowledge of the roll-off factors allows for efficient noise reduction by applying the fitting matched filter at the receiver and reduces intersymbol interference at the correct sampling instants.

C. LITERATURE REVIEW AND CONTRIBUTION

1) POWER ESTIMATION

To the knowledge of the authors, the explicit estimation of the carrier powers of cochannel signals that are comparable to the PCMA signal is rarely treated in the literature. Several works that propose detection schemes for PCMA or cochannel signals include implicit parameter estimation by decision-aided adaptation of the coefficients of the channel model, e.g. by employing the per-survivor processing (PSP)-algorithm [6] or alternating optimization [7]. However, they require an initialization of the estimate of the channel or its parameters, respectively, which is not explicitly provided. In [8], a scheme is proposed that estimates the carrier powers jointly with classifying the carrier modulation constellations, based on the minimum squared error fitting of statistical

features. Here, a set of measured and hypothetical cyclic cumulant features is used, where the latter are conditioned on the modulations and the carrier powers. The considered set is chosen to be distinctive with respect to different modulation constellations and includes cyclic cumulants of orders up to eight. Yet, cyclic cumulants of such high orders are not required for power estimation in the case of various relevant modulation constellations. At the same time, they are sensitive with respect to estimation errors that impact the performance of estimation of the carrier powers. However, the authors do not provide an explicit evaluation of the power estimation performance and their focus is on the modulation classification accuracy. In [9], the authors present a method for estimation of the amplitudes of the individual signals in a cochannel scenario. Yet, unequal symbol rates of the individual SC signals are assumed, which is incompatible to the assumptions we apply for our considerations here. Also, there are approaches for the direct estimation of the SNR that exploit the structures of the fourth and second-order moments of the received signal [10]. However, typically they cannot be applied to the PCMA case directly. This is because, in the case of cochannel signals, the fourth-order moment of the sum signal is scaled by the squared total power of the noise-free signals, but the powers of both data-carrying signals impact the fourth-order moment individually. If instead the power imbalance of the two carriers is known, an equivalent expression of the fourth-order statistics of the received signal may derived which may be exploited for SNR estimation. In principle, the power imbalance of the SC signals within the PCMA signal can be estimated [4] if the roll-off factors are identical or assumed to be known. However, if the knowledge of the roll-off factors can be assumed, the individual powers may be estimated using the method presented in this paper and the derivation of the imbalance becomes unnecessary. Other methods for direct SNR estimation in the case of SC signal are summarized and compared e.g. in [11]. Here, intersymbol interference-free reception is assumed, which is enabled by knowledge of the carrier frequency and symbol clock and a corresponding demodulation and sampling. While the respective signal parameters may also be acquired through blind estimation in the PCMA case (cf. [12], [13]), compensation of the respective frequency and symbol timing offsets in general cannot be fulfilled for both carrier signals simultaneously. Thus, the corresponding SNR estimation approaches are not applicable to PCMA signals.

The noise power estimation that is introduced in [4] relies on the estimation of the noise autocorrelation which is determined by the characteristics of the receiver input filter. In [4], it is assumed that the filter has a bandwidth larger than the bandwidth of the received signal. Consequently, out-of-band noise is included in the signal at the filter output, which is exploited for the estimation of the noise power spectral density. In contrast, in many practical cases, different satellite signals are narrowly placed in frequency bands next to each other without significant guard bands between them. Here, the receiver input filter bandwidth may not be larger than the bandwidth of the signal of interest and no out-of-band noise is present at the filter output. As we adopt the practical assumptions stated above, the approach of [4] is not employed in this paper.

CONTRIBUTION

Here, we present an approach for estimating the respective powers of the individual SC signals that form the PCMA signal. It exploits the separability of certain higher-order cyclostationary statistics of the two carriers. This separability is based on the assumption that their carrier frequency offsets (CFOs) are non-identical and sufficiently different in the sense of the given measurement resolution, while the two SC signals share the same frequency band and hence, the same nominal carrier frequency. The statistics may be estimated based on the received PCMA signal, yet the order of the required statistics for modulation schemes like 8-ary phase-shift keying (8PSK) renders the estimation of the respective statistics error-prone for limited signal segment lengths. In order to circumvent this problem, we propose an alternative scheme for the inference of the carrier powers for which the order of the estimated statistics is limited to six. The estimation of the desired statistics requires prior information on the CFOs and the symbol rate of the SC signals, respectively. We assume the information on the required parameters to be obtained by blind estimation schemes (e.g. [12]) that are employed precedent to power estimation processing considered in the present paper. We also compare our presented schemes to the power estimation scheme that is a part of the modulation classification scheme of [8].

2) ROLL-OFF FACTOR ESTIMATION

To the best of our knowledge, an explicit estimation of the roll-off factors of the carrier signals in a blind receiver of a PCMA signal has not been investigated by other authors in the literature before. The scheme proposed in [14] estimates the time-averaged power spectral density (PSD_0) of a received SC signal and computes its inverse Fourier transform for characterization of the raised-cosine pulse shape. Here, the ratio of the heights of its main lobe and first side lobe gives rise to the roll-off factor of the transmit pulse. In general, only for SC signals the raised-cosine pulse is directly observable in the inverse Fourier transform of the PSD_0 estimate. Hence, the scheme cannot be straightforwardly extended to the model of a PCMA scenario. Similarly, the inference of the roll-off factor from the ratio of the peaks of the squared magnitude of an estimate of the cyclic autocorrelation function of the received signal according to [15] may not be directly applied here, since the individual carriers share the same symbol rate and their cyclic autocorrelations interfere with each other. Another method that is outlined in [16] is based on the minimization of the squared distance of the PSD_0 of the noise-free receive signal conditioned on the hypothetical roll-off factor to the PSD_0 estimate of the received signal. However, this approach requires explicit knowledge of the PCMA signal power levels and power spectral density of the noise. Because their estimation is carried out after inference

of the roll-off factors in our receiver model, this requirement is prohibitive for the practical application of the scheme.

CONTRIBUTION

We advocate an alternative scheme employing a standard artificial neural network (ANN) structure which is adapted to roll-off factor estimation by a training process using a data set of estimates of the PSD_0 of received PCMA signals. We design the ANN such that it provides sufficiently accurate estimates at relatively low complexity that allow for the subsequent usage of the presented power estimation schemes. Our experiments indicate that the performance of the employed ANN is close to that of the case where the ground truth values of the roll-off factors are provided to the subsequent power estimation scheme. Here, the training data is generated from simulated received signals. A cross-verification of the ANN based roll-off factor estimator with measured real world data is desirable but not within the scope of this paper.

In contrast to previously proposed schemes, the ANN based approach is specifically tailored to the scenario of co-channel signals by using examples of PCMA signals during the training phase. Furthermore, no explicit knowledge of the CFOs or power spectral density of the noise is required in order to exploit the spectral features.

D. PAPER STRUCTURE

The remaining part of the paper is organized as follows. The assumptions on the considered system and its mathematical model are described in Section II. In Section III, the utilized cyclostationary quantities and their respective estimators are introduced, and different approaches for the estimation of the carrier and noise powers are derived. In Section IV we give the structure and training setup of an ANN based estimator that provides the necessary knowledge of the roll-off factors to enable the deployment of the power estimators. Numerical evaluations and comparisons of the presented approaches are given in Section V. We conclude the paper in Section VI.

II. SYSTEM MODEL

The equivalent complex baseband representation of the linear digitally modulated transmit signals corresponding to the two carrier signals that are captured at the blind receiver is given by

$$s_i(t) = \sum_{k=-\infty}^{+\infty} a_{i,k}\, g_i(t - kT), \tag{1}$$

where $i \in \{1, 2\}$ denotes the carrier index, k stands for the symbol interval index and T represents the symbol period which is identical for both carriers. The symbol $a_{i,k}$ of carrier i and symbol interval k is an element of the respective modulation constellation of carrier i given by the set $\mathbb{A}_i$ with zero-mean and unit mean energy. All symbols are stochastically independent with respect to i and k and identically distributed with respect to k. The transmit pulse shape denoted by $g_i(t)$ is of root-raised-cosine type, parameterized by the individual roll-off factor ρ_i. The pulses $g_i(t)$ have unit energy, i.e., $\int_{-\infty}^{\infty} |g_i(t)|^2 \,\mathrm{d}t = 1$.

The transmitters are generally not synchronized with each other or with the receiver hardware, and the wireless channels from the GSs to the possibly non-stationary satellite are distinct, respectively. Accordingly, each carrier signal of index i is affected by individual carrier frequency and phase offsets f_i and ϕ_i, and symbol timing offsets τ_i. The satellite transponder adds up the received uplink signals and retransmits the sum signal in the downlink. This downlink signal is then taken up by the blind receiver on earth and is corrupted by additive noise. Hence, the received PCMA signal at the blind receiver is modeled as

$$r(t) = \sum_{i=1}^{2} \sqrt{E_{\mathrm{S},i}}\, e^{\mathrm{j}(2\pi f_i t + \phi_i)} s_i\,(t - \tau_i) + w(t), \tag{2}$$

where the received energy per symbol $E_{\mathrm{S},i}$ of carrier i reflects channel attenuation effects as well as possible power allocations with respect to each carrier. A lowpass filter at the input of the blind receiver suppresses interference from adjacent channels in the equivalent complex baseband domain and leaves the PCMA signal within its passband free of any distortion by filtering. At the same time, it limits the bandwidth and power of the complex additive white Gaussian noise (AWGN) with power spectral density N_0 at the receiver input resulting in the effective noise $w(t)$.

We restrict the domains of the carrier phases and symbol timing offsets to $\phi_i \in [0, 2\pi)$ and $\tau_i \in (-T/2, T/2]$, respectively, for convenience of notation and without restricting generality, here. A limitation of the magnitudes of the carrier frequency offsets to $|f_i| \leq f_{\max}$ is assumed, which may be derived from hardware and channel specifications in practice. This further renders the assumption of the lowpass filter to leave the PCMA signal undistorted practical.

The power estimators in this paper rely on the knowledge of the symbol rate $1/T$ and the carrier frequency offsets f_i, which we assume to be retrieved by adequate prior processing, using e.g. the estimators proposed in [12]. Furthermore, both modulation schemes of the respective carriers are assumed to be known, e.g. via neural network based co-channel classification schemes [17].

In a practical blind receiver, the received signal is processed digitally after T_s-spaced sampling. The sampling frequency $1/T_\mathrm{s}$ is chosen large enough such that the relevant statistical features may be estimated without any corruption due to aliasing. Here, the knowledge of the symbol rate $1/T$, $f_{\max}$ and the range of possible roll-off factors is exploited in order to determine the largest expected bandwidth of the received signal.

III. CARRIER AND NOISE POWER ESTIMATORS

In this section, we first establish the cyclostationary properties that are employed for the proposed estimation schemes. Based on these properties, we subsequently derive estimators for energy per symbol of the carriers for different cases of modulations of the carriers. Here, the estimation of the energy

per symbol for each carrier is equivalent to carrier power estimation for known symbol period T. Furthermore, noise power estimation is addressed.

A. CYCLIC MOMENTS AND CYCLIC CUMULANTS OF PCMA SIGNALS

The pth-order moment including q conjugations, $m_{r,(p,q)}(t) = \mathrm{E}\{(r(t))^{p-q}(r^*(t))^q\}$ of a PCMA received signal $r(t)$ is generally time-varying. For appropriate p and q, $\mathrm{E}\{a_{i,k}^{p-q}(a_{i,k}^*)^q\} \neq 0$ for at least one i, and $m_{r,(p,q)}(t)$ admits a series expansion

$$m_{r,(p,q)}(t) = \sum_{\alpha \in \mathcal{A}_{r,(p,q)}} M_{r,(p,q)}(\alpha) e^{\mathrm{j}2\pi\alpha t}, \tag{3}$$

where $\mathcal{A}_{r,(p,q)}$ is the set of so-called cycle frequencies α for which the coefficients

$$M_{r,(p,q)}(\alpha) = \lim_{Z\to+\infty} \frac{1}{Z} \int_{-Z/2}^{Z/2} m_{r,(p,q)}(t) e^{-\mathrm{j}2\pi\alpha t}\, \mathrm{d}t, \tag{4}$$

which are referred to as (p, q) cyclic moments at cycle frequency α, are nonzero.

The (p, q) cumulant of $r(t)$, i.e., the pth-order cumulant of $r(t)$ with q complex conjugations, can be calculated using moments of orders up to p by the expression

$$c_{r,(p,q)}(t) = \sum_{b=1}^{B_p} (-1)^{\lambda_b - 1} (\lambda_b - 1)! \prod_{l=1}^{\lambda_b} m_{r,(p_{b,l},q_{b,l})}(t), \tag{5}$$

where the sum is over all B_p partitions $\mathcal{P}_b$ ($b = 1, \ldots, B_p$), of a set $\mathcal{X}_{(p,q)}$ containing $(p - q)$ times $r(t)$ and q times $r^*(t)$. Each partition contains a respective number λ_b of non-empty subsets $\mathcal{S}_{b,l}$ ($l = 1, \ldots, \lambda_b$), i.e., $\mathcal{P}_b = \{\mathcal{S}_{b,l}\}_{l=1}^{\lambda_b}$. Moreover, each $\mathcal{S}_{b,l}$ of size $|\mathcal{S}_{b,l}| = p_{b,l}$ contains $(p_{b,l} - q_{b,l})$ times $r(t)$ and $q_{b,l}$ times $r^*(t)$, such that every element of $\mathcal{X}_{(p,q)}$ is included in exactly one of the λ_b subsets $S_{b,l}$ for every b and therefore $\bigcup_{l=1}^{\lambda_b} \mathcal{S}_{b,l} = \mathcal{X}_{(p,q)}$.

Assuming that $c_{r,(p,q)}(t)$ is not identical to zero for all t, it admits a series expansion

$$c_{r,(p,q)}(t) = \sum_{\beta \in \mathcal{B}_{r,(p,q)}} C_{r,(p,q)}(\beta) e^{\mathrm{j}2\pi\beta t} \tag{6}$$

with cycle frequencies $\beta \in \mathcal{B}_{r,(p,q)}$ for which the coefficients

$$C_{r,(p,q)}(\beta) = \lim_{Z\to+\infty} \frac{1}{Z} \int_{-Z/2}^{Z/2} c_{r,(p,q)}(t) e^{-\mathrm{j}2\pi\beta t}\, \mathrm{d}t, \tag{7}$$

which are referred to as cyclic cumulants, are nonzero.

The (p, q) cyclic cumulant of a transmit signal $s_i(t)$ can be derived to

$$C_{s_i,(p,q)}(\beta) = \begin{cases} \dfrac{c_{a_i,(p,q)}}{T} G_{i,p}(\beta) & \text{for } \beta \in \mathcal{B}_{s_i,(p,q)} \\ 0 & \text{else} \end{cases} \tag{8}$$

where $G_{i,p}(f) = \int_{-\infty}^{+\infty} [g_i(t)]^p e^{-\mathrm{j}2\pi f t}\, \mathrm{d}t$, assuming real $g_i(t)$ $\forall t, i$. Furthermore, $c_{a_i,(p,q)}$ denotes the (p, q) cumulant of the symbols $a_{i,k}$, which is determined by the modulation constellation $\mathbb{A}_i$ and identical for all k. Note that, if for the particular modulation constellation $\mathbb{A}_i$ the cumulant of the constellation equals zero, e.g. $c_{a_i,(2,0)} = 0$ if $\mathbb{A}_i$ is of any phase-shift keying (PSK) constellation of order larger than 2, then the set of cycle frequencies $\mathcal{B}_{i,(p,q)}$ is empty. Provided that $c_{a_i,(p,q)} \neq 0$, the set of cycle frequencies of the (p, q) cyclic cumulant of carrier $s_i(t)$, which is denoted by $B_{s_i,(p,q)}$, is composed of integer multiples of $1/T$ [18]. In particular, if transmit pulses $g_i(t)$ of bandwidth B_{g_i} are assumed, it can be shown using fundamental properties of the Fourier transform that the bandwidth of $G_{i,p}(\beta)$ is pB_{g_i}, i.e. $G_{i,p}(f) \neq 0$ for $|f| \leq pB_{g_i}$. As a consequence, the set of cycle frequencies reduces to $\mathcal{B}_{s_i,(p,q)} = \{u_i/T \mid |u_i| \leq pB_{g,i}T\}$, for $i = 1, 2$, here.

Since the additive thermal noise is stationary, hence, the (p, q) cyclic cumulant of $w(t)$ is given by

$$C_{w,(p,q)}(\beta) = \begin{cases} c_{w,(p,q)} & \text{for } \beta = 0 \\ 0 & \text{else.} \end{cases} \tag{9}$$

Hence, the only "cycle" frequency that is present in the noise is DC. Furthermore, since the noise is Gaussian, zero-mean and circularly symmetric, $c_{w,(p,q)} \neq 0$ only for $(p, q) = (2, 1)$.

A pivotal property of cumulants is that the cumulant of the sum of independent signals equals the sum of the respective cumulants of the signals [19]. Acknowledging this property and regarding the definition of the PCMA signal (2) allows to derive the (p, q) cyclic cumulant of the PCMA received signal, i.e.,

$$C_{r,(p,q)}(\beta) = \sum_{i=1}^{2} E_{\mathrm{S},i}^{p/2} C_{s_i,(p,q)}(\gamma_i) e^{\mathrm{j}(-2\pi\gamma_i\tau_i + (p-2q)\phi_i)} + C_{w,(p,q)}(\beta), \tag{10}$$

where $\gamma_i = \beta - (p - 2q)f_i$ is used for convenience in notation. Considering the composition of the PCMA received signal in (2), the set of cycle frequencies $\mathcal{B}_{r,(p,q)}$ of $c_{r,(p,q)}(t)$ can be determined as $\mathcal{B}_{s_i,(p,q)} + (p - 2q)f_i$, $i = 1, 2$ and DC for the noise cumulant in the case of $(p, q) = (2, 1)$. Here, the cycle frequency sets of the two single-carrier signals are non-empty sets only if the cumulants of the respective modulation constellations $c_{a_i,(p,q)}$ are nonzero for the respective values of (p, q). However, the expression (10) holds even if $c_{a_i,(p,q)} = 0$ for any i or $c_{w,(p,q)} = 0$ and the corresponding sets of cycle frequencies are empty. In that case, the respective contribution in (10) may be set to zero.

We now focus on a first special case of the cyclic cumulants, i.e., the $(p, 0)$ cyclic cumulants with no conjugations. Choosing $(p, q) = (p, 0)$ and restricting the cycle frequencies to $\beta \in \mathcal{B}_{r,(p,q),i} = \{pf_i + u_i/T \mid |u_i| \leq pB_{g,i}T\}$ for $i = 1, 2$, (10) simplifies to

$$C_{r,(p,0)}(\beta) = E_{\mathrm{S},i}^{p/2} C_{s_i,(p,0)}(\gamma_i) e^{\mathrm{j}(-2\pi\gamma_i\tau_i + p\phi_i)}, \tag{11}$$

where $f_1 \neq f_2$ has been assumed to ensure that the cyclic cumulants are selective with respect to a single respective carrier. Further, it is exploited that the $(p, 0)$ cumulants of the zero-mean circularly symmetric complex noise are zero for all p.

The second special case we investigate here are the cyclic cumulants for $(p, q) = (p, p/2)$ for even p. In this case, the cycle frequency set simplifies to $\mathcal{B}_{r,(p,p/q)} = \{u/T \mid u \in \mathbb{Z}, |u| < \max_i(pB_{g,i}T)\}$. Using $q = p/2$ conjugations in (10) yields

$$C_{r,(p,\frac{p}{2})}\left(\frac{u}{T}\right) = \sum_{i=1}^{2} E_{\mathrm{S},i}^{p/2} C_{s_i,(p,\frac{p}{2})}\left(\frac{u}{T}\right) \cdot e^{-\mathrm{j}2\pi(u/T)\tau_i} + C_{w,(p,q)}\left(\frac{u}{T}\right) \tag{12}$$

which is nonzero for $|u| < \max_i \left(pB_{g,i}T\right)$.

The processing in a practical receiver is carried out digitally using a segment of the sampled received signal

$$r[n] = r\left(nT_\mathrm{s}\right) \tag{13}$$

with a sampling rate of $1/T_\mathrm{s}$ chosen large enough to avoid any aliasing effects over the course of the subsequent processing. For the one-sided bandwidth B of the receiver input filter, the condition $1/T_\mathrm{s} > 2pB$ is generally sufficient considering (p, q) moments and cumulants. It is obvious that the (p, q) moments of the discrete-time received signal $\tilde{m}_{r,(p,q)}[n] = \mathrm{E}\left\{(r[n])^{p-q}\,(r^*[n])^q\right\} = m_{r,(p,q)}(t)\big|_{t=nT_\mathrm{s}}$ correspond to the respective (p, q) moments of the continuous-time received signal at the particular sampling time instances. In the same way, the (p, q) cumulants of the discrete-time signal $r[n]$ correspond to the (p, q) cumulants of the continuous time signal, i.e., $\tilde{c}_{r,(p,q)}[n] = c_{r,(p,q)}(t)\big|_{t=nT_\mathrm{s}}$. As for the continuous-time case, the moments and cumulants of the discrete-time signal admit series expansions whose coefficients are the cyclic moments $\tilde{M}_{r,(p,q)}(\tilde{\alpha})$ and cyclic cumulants $\tilde{C}_{r,(p,q)}(\tilde{\beta})$, respectively. The latter relate to their continuous-time counterparts by [20, Ch. 3,4]

$$M_{r,(p,q)}(\alpha) = \tilde{M}_{r,(p,q)}(\tilde{\alpha})\Big|_{\tilde{\alpha}=\alpha T_\mathrm{s}}, \tag{14}$$

$$C_{r,(p,q)}(\beta) = \tilde{C}_{r,(p,q)}(\tilde{\beta})\Big|_{\tilde{\beta}=\beta T_\mathrm{s}}, \tag{15}$$

where $\alpha \in \mathcal{A}_{r,(p,q)}$, $\beta \in \mathcal{B}_{r,(p,q)}$. Hence, estimates of the cyclic moments $M_{r,(p,q)}(\alpha)$ of the continuous-time signal can be obtained by estimating the cyclic moments $\tilde{M}_{r,(p,q)}(\alpha T_\mathrm{s})$ of the corresponding discrete-time signal. The latter are obtained from the samples of a finite-length measurement of the received signal by

$$\hat{\tilde{M}}_{r,(p,q)}(\tilde{\alpha}) = \frac{1}{2N+1} \sum_{n=-N}^{N} (r[n])^{p-q} \left(r^*[n]\right)^q e^{-\mathrm{j}2\pi\tilde{\alpha}n}. \tag{16}$$

Such estimate is asymptotically unbiased and consistent [21].

In order to derive an estimator for the cyclic (p, q) cumulants using the observed signal segment, the relation of the cyclic cumulants to the cyclic moments of orders $p' \leq p$ is exploited. Using the relation between the cumulants and the moments in the time domain as given in (5) together with the relation between the cumulants and the cyclic cumulants in (7) yields the expression of the cyclic cumulants via the cyclic moments,

$$C_{r,(p,q)}(\beta) = \sum_{b=1}^{B_p} K_b \sum_{\sum_{l=1}^{\lambda_b} \gamma_{b,l} = \beta} \prod_{l=1}^{\lambda_b} M_{r,(p_{b,l},q_{b,l})}(\gamma_{b,l}), \tag{17}$$

where we use the definition $K_b = (-1)^{\lambda_b - 1}\,(\lambda_b - 1)!$ for convenience. Here, for each partition index b, the inner sum is over all combinations of cycle frequencies $\gamma_{b,l}$ of moments $m_{r,(p_{b,l},q_{b,l})}(t)$ for which $M_{r,(p_{b,l},q_{b,l})}(\gamma_{b,l}) \neq 0$, respectively, and sum up to β. With this, estimates for the cyclic cumulants $\hat{C}_{r,(p,q)}(\beta)$ are obtained by replacing $M_{r,(p_{b,l},q_{b,l})}(\gamma_{b,l})$ in (17) by the corresponding estimates $\hat{M}_{r,(p_{b,l},q_{b,l})}(\gamma_{b,l}) = \hat{\tilde{M}}_{r,(p_{b,l},q_{b,l})}(\gamma_{b,l}T_\mathrm{s})$.

B. CARRIER POWER ESTIMATION

1) APPROACH USING $C_{r,(p,0)}(pf_i + u_i/T)$

Rearranging the carrier selective representation (11) for cycle frequencies $\beta \in \mathcal{B}_{r,(p,q),i}$ for $i = 1, 2$ yields

$$E_{\mathrm{S},i}^{p/2} = \frac{C_{r,(p,0)}(\beta)\, e^{\mathrm{j}(2\pi\gamma_i\tau_i - p\phi_i)}}{C_{s_i,(p,0)}(\beta - pf_i)} = \frac{\left|C_{r,(p,0)}(\beta)\right|}{\left|C_{s_i,(p,0)}(\beta - pf_i)\right|}, \tag{18}$$

where for deriving the second equation it is recognized that the energy per symbol is equal to its absolute value. If the modulation scheme and the pulse shape $g_i(t)$ (or, respectively, the roll-off factor ρ_i that parameterizes it) are known, $c_{a_i,(p,0)}$ and $G_{i,p}(\beta)$ can be derived, respectively. Thus, $C_{s_i,(p,0)}(\beta)$ can be determined (cf. (8)), where also the known symbol rate $1/T$ is used. Together with an estimate $\hat{C}_{r,(p,q)}(\beta)$ of the $(p, 0)$ cyclic cumulant at cycle frequency $\beta \in \mathcal{B}_{r,(p,q),i}$ for $i = 1, 2$, the energy per symbol of carrier i can be estimated as

$$\hat{E}_{\mathrm{S},i} = \left(\frac{\left|\hat{C}_{r,(p,0)}(\beta)\right| \cdot T}{\left|c_{a_i,(p,0)}\right| \left|G_{i,p}(\beta - pf_i)\right|}\right)^{2/p}. \tag{19}$$

Obviously, $c_{a_i,(p,0)} \neq 0$ needs to be fulfilled for the estimator, i.e., p has to be greater than or equal to the order of non-circularity of the respective $\mathbb{A}_i$. Note that the number of required calculations and the complexity that comes with computing the estimates can be kept relatively low if p is chosen to be the lowest possible order, i.e., the order of non-circularity. This is because in this case all involved moments of orders $p' < p$ in (17) are known to be zero and the $(p, 0)$ cumulant is equal to the $(p, 0)$ moment.

2) APPROACH USING $C_{r,(6,3)}(\frac{u}{T})$ AND $C_{r,(4,2)}(\frac{u}{T})$

It turns out in experimental evaluations that the estimates of cumulants of high orders p suffer from large estimation variances. This also becomes apparent in the presented numerical results in Section V. As an example, $p = 8$ needs

to be chosen for 8PSK modulation. This case requires a large length of the signal segment for obtaining $\hat{C}_{r,(8,0)}\,(8f_i)$ with sufficient accuracy for a high-quality power estimation according to (19). Therefore, we derive an alternative procedure to estimate the carrier powers that employs $(p, p/2)$ cumulants of lower orders $p < 8$, which are nonzero for also the frequently used higher-order PSK or quadrature amplitude modulation (QAM) schemes. The particular choice of the cyclic cumulants whose estimates serve as features from which the carrier powers are inferred, is based on the following considerations. For the reasons stated above, we target to utilize estimates of cumulants of order $p < 8$. While the $(p, p/2)$ cumulants are nonzero for any other PSK and QAM modulations, they are the only cumulants with $p < 8$ that are nonzero for 8PSK. From (12) we observe that the cyclic cumulants for cycles $\beta \neq 0$ for which $C_{r,(p,p/2)}(\beta) \neq 0$ holds depend on the symbol timing offsets τ_i for $i = 1, 2$. Although the symbol timing offsets may be estimated [13], we prefer features that do not require their respective knowledge, as the values of the symbol timings may themselves be subject to estimation errors. Furthermore, the magnitude of $C_{r,(p,p/2)}(\beta) \neq 0$ for $\beta \neq 0$ can in general be attenuated by the incoherent summation in (cf. (12)) which may result in destructive superposition of the respective contributions of the two SC signals to this cyclic cumulant. Also, the magnitude of the respective cyclic cumulants $C_{r,(p,p/2)}(\beta) \neq 0$ at $\beta = |u|/T$, $u = 1, 2, \ldots$ is determined by $G_{i,p}(u/\beta)$, i.e., the p-fold convolution of the Fourier transform of the transmit pulse, which may take on small values for small roll-off factors ρ_i. Consequently, we expect the cyclic cumulants $C_{r,(p,p/2)}(\beta) \neq 0$ for $\beta \neq 0$ to be more susceptible to estimation errors. Therefore, we restrict the set of considered $(p, p/2)$ cyclic cumulants to those of cycle $\beta = 0$. With respect to the remaining cyclic cumulants, we exclude $C_{r,(2,1)}(0)$, which corresponds to the time-averaged power of the received signal, as it also contains contributions of the noise, of which we assume the power to be unknown at this stage of the processing in the blind receiver. As a result, the two cyclic cumulants $C_{r,(6,3)}(0)$ and $C_{r,(4,2)}(0)$ are employed as features for our alternative approach to the estimation of the carrier powers.

For $p \in \{4, 6\}$, we observe the corresponding cyclic cumulant expressions

$$C_{r,(p,p/2)}\,(0) = \frac{1}{T}\sum_{i=1}^{2} \underbrace{c_{a_i,(p,p/2)} G_{i,p}(0)}_{A_{i,(p,p/2)}} E_{\mathrm{S},i}^{p/2}, \tag{20}$$

and introduce the definition $A_{i,(p,q)} = c_{a_i,(p,q)} G_{i,p}(0)$ for convenience in notation. Obviously, the cyclic cumulants in (20) contain contributions of both individual carriers such that the respective powers may not be inferred from only one cyclic cumulant. In order to obtain an expression that depends on only a single variable, we employ the quotient

$$Y = \frac{\left(C_{r,(6,3)}\,(0)\cdot T\right)^2}{\left(C_{r,(4,2)}\,(0)\cdot T\right)^3} = \frac{\left(A_{1,(6,3)}E_{\mathrm{S},1}^3 + A_{2,(6,3)}E_{\mathrm{S},2}^3\right)^2}{\left(A_{1,(4,2)}E_{\mathrm{S},1}^2 + A_{2,(4,2)}E_{\mathrm{S},2}^2\right)^3}$$

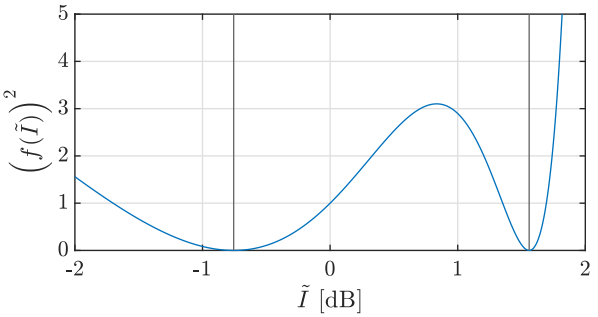

FIGURE 1. Example of a normalized version of the fitting function with two minima. The two vertical lines point out the found minima.

$$= \frac{\left(A_{1,(6,3)}I^3 + A_{2,(6,3)}\right)^2}{\left(A_{1,(4,2)}I^2 + A_{2,(4,2)}\right)^3}, \tag{21}$$

where we have used the power imbalance of the two carriers, $I = E_{\mathrm{S},1}/E_{\mathrm{S},2}$, which serves as solitary parameter to be estimated in the first step of this approach.

The formulation (21) can be rearranged to a polynomial equation in I of order six. The preknowledge $I \in \mathbb{R}, I > 0$ along with information on the largest expected carrier power imbalance of the system governed by the specific application scenario, e.g. $\left|10\log_{10}(I)\right| < 1\,\mathrm{dB}$, can be exploited for its solution. By restricting the domain of I according to the considerations above, we observe that we can solve the polynomial equation for the correct I numerically in all considered cases.

A practical receiver is restricted to use estimates of the cyclic cumulants and roll-offs for any of the statistical estimators described above. Hence, we need to replace Y or $C_{r,(p,q)}(\beta)$ and also $G_{i,p}(\beta)$ or $A_{i,(p,q)}$ by their respective estimates $\hat{Y}$ or $\hat{C}_{r,(p,q)}(\beta)$ and $\hat{G}_{i,p}(\beta)$ or $\hat{A}_{i,(p,q)}$. Consequently, instead of solving (21), we therefore decide to search for those values of I that minimize the squared error for fitting (21). For this purpose, we develop (21) as

$$\frac{\left(C_{r,(6,3)}\,(0)\cdot T\right)^2}{\left(C_{r,(4,2)}\,(0)\cdot T\right)^3} - Y = 0 \tag{22}$$

whose expansion yields the function

$$\begin{aligned} f(\tilde{I}) = &\left(A_{1,(6,3)}^2 - A_{1,(4,2)}^3 Y\right)\tilde{I}^6 - \left(3A_{1,(4,2)}^2 A_{2,(4,2)} Y\right)\tilde{I}^4 \\ &+ \left(2A_{1,(6,3)}A_{2,(6,3)}\right)\tilde{I}^3 - \left(3A_{1,(4,2)}A_{2,(4,2)}^2 Y\right)\tilde{I}^2 \\ &+ \left(A_{2,(6,3)}^2 - A_{2,(4,2)}^3 Y\right) \end{aligned} \tag{23}$$

which equals zero for $\tilde{I} = I$. Supported by our numerical investigations, we find that $(f(I))^2$ has two minima for real I. Examples for the two respective cases are shown in Fig. 1 and Fig. 2.

In the case of a single minimum we find the estimate for the carrier power imbalance numerically as

$$\hat{I} = \underset{I}{\operatorname{argmin}}\,(f(I))^2, \tag{24}$$

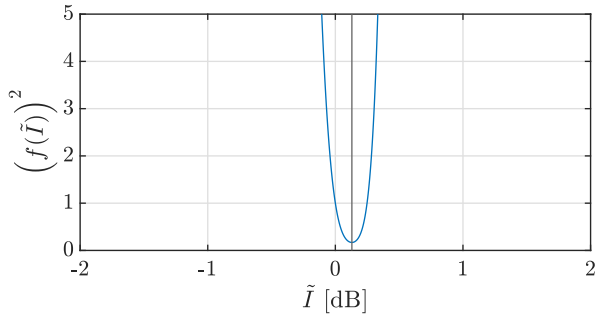

FIGURE 2. Example of a normalized version of the fitting function with one minimum. The vertical line points out the found minimum.

and can subsequently derive estimates for the respective energies per symbol $E_{\mathrm{S},i}$ for $i = 1, 2$ by

$$\hat{E}_{\mathrm{S},2} = \sqrt{\hat{C}_{r,(4,2)}(0) \cdot T / \left(A_{1,(4,2)}\hat{I}^2 + A_{2,(4,2)}\right)}, \tag{25}$$

$$\hat{E}_{\mathrm{S},1} = \hat{E}_{\mathrm{S},2} \cdot \hat{I}. \tag{26}$$

In the case of two local minima, we find both corresponding solutions for $\tilde{I}$ and respectively denote them by $\hat{I}_l$ for $l \in \{1, 2\}$. For each solution for the imbalance we derive a solution for $E_{\mathrm{S},1}$ and $E_{\mathrm{S},2}$, respectively, i.e.,

$$\hat{E}_{\mathrm{S},2,l} = \sqrt{\hat{C}_{r,(4,2)}(0) \cdot T / \left(A_{1,(4,2)}\hat{I}_l^2 + A_{2,(4,2)}\right)}, \tag{27}$$

$$\hat{E}_{\mathrm{S},1,l} = \hat{E}_{\mathrm{S},2,l} \cdot \hat{I}_l. \tag{28}$$

Finally, we choose

$$(\hat{E}_{\mathrm{S},1}, \hat{E}_{\mathrm{S},2}) = (\hat{E}_{\mathrm{S},1,\hat{l}}, \hat{E}_{\mathrm{S},2,\hat{l}}), \tag{29}$$

$$\hat{l} = \underset{l\in\{1,2\}}{\operatorname{argmin}} \sum_{i=1}^{2} \left(\hat{E}_{\mathrm{S},i,l} - \left(\frac{\left|\hat{C}_{r,(p,0)}(\beta)\right| \cdot T}{|A_{i,(p,0)}|} \right)^{2/p} \right)^2, \tag{30}$$

which means that we use that solution $(\hat{E}_{\mathrm{S},1,l}, \hat{E}_{\mathrm{S},2,l})$ that has the smaller Euclidean distance to the possibly relatively noisy estimate that is obtained via the approach of (19).

3) MIXED APPROACH

If only one of the carriers is 8PSK-modulated and the other one uses a modulation of non-circularity order lower than eight, a simplified approach can be derived that provides an enhanced accuracy for estimating the power of the 8PSK-modulated carrier using the cumulants $C_{r,(p,0)}(f_i)$ and $C_{r,(4,2)}(0)$. Without loss of generality, we assume that the carrier with index $i = 2$ is 8PSK-modulated and the carrier with index $i = 1$ uses a modulation with lower non-circularity order, e.g., quadrature PSK (QPSK). Here, we exploit the fact that $C_{r,(p,0)}(pf_1)$ can be more accurately estimated for $p < 8$, i.e., $p = 2, 4$ than for $p = 8$. For this purpose, the estimate $\hat{E}_{\mathrm{S},1}$ is obtained first using $\hat{C}_{r,(o_1,0)}(o_1 f_1)$ along with (19), where o_i is the order of non-circularity of the carrier $i = 1, 2$, and here $o_1 < 8$. From (20) with $p = 4$ we find that

$$E_{\mathrm{S},2} = \sqrt{\frac{C_{r,(4,2)}(0)\, T - c_{a_1,(4,2)} G_{1,4}(0) E_{\mathrm{S},1}^2}{c_{a_2,(4,2)} G_{2,4}(0)}}, \tag{31}$$

and replace $C_{r,(4,2)}(0)$ and $E_{\mathrm{S},1}^2$ in (31) by their respective estimates $\hat{C}_{r,(4,2)}(0)$ and $\hat{E}_{\mathrm{S},1}$ to obtain an estimate $\hat{E}_{\mathrm{S},2}$ for $E_{\mathrm{S},2}$.

C. NOISE POWER ESTIMATION

After having estimated the energies per symbol of both carriers, a straightforward approach for estimating the power of the noise contained in the PCMA received signal is adopted. As pointed out above, the noise power is represented in the time-averaged power of the received signal, i.e., the $C_{r,(2,1)}(0)$ cyclic cumulant, which is obtained from (20) for $(p, q) = (2, 1)$ and $\beta = 0$ with (9) as

$$\begin{aligned} C_{r,(2,1)}(0) &= \sum_{i=1}^{2} E_{\mathrm{S},i} C_{s_i,(2,1)}(0) + c_{w,(2,1)} \\ &= \frac{1}{T} \sum_{i=1}^{2} E_{\mathrm{S},i} + c_{w,(2,1)}, \end{aligned} \tag{32}$$

where the second equation results from inserting the expression for $C_{s_i,(2,1)}(\beta)$ of (8) and acknowledging that the modulation symbols and the transmit pulses are defined to have unit variance $c_{a_i,(2,1)} = 1$ and unit energy $G_{i,2}(0) = 1$, $i = 1, 2$, respectively.

Hence, using the obtained estimates $\hat{E}_{\mathrm{S},i}$ together with an estimate for the received PCMA signal power $\hat{C}_{r,(2,1)}(0)$ yields the noise power estimate

$$\hat{c}_{w,(2,1)} = \hat{C}_{r,(2,1)}(0) - \frac{1}{T} \sum_{i=1}^{2} \hat{E}_{\mathrm{S},i}. \tag{33}$$

Note that the variance of the estimates of the energies per symbol may result in very small positive or even negative values for $\hat{c}_{w,(2,1)}$. In a practical receiver, this noise variance estimate may be biased by setting up a lower threshold below which it is not allowed to drop. This limit can be derived from side-knowledge about the application scenario or properties of the receiver hardware. We do not consider such approach here, since it does not affect the essence of our scheme and is highly dependent on the particular use case.

IV. NEURAL NETWORK FOR ROLL-OFF FACTOR ESTIMATION

With respect to the power estimation approaches introduced above, it is obvious that the knowledge of the transmit pulse shapes, or equivalently, the roll-off factors that parameterize them, is essential as the selected cyclic cumulant features depend on the frequency representations of the pth powers of the transmit pulses, i.e., $G_{i,p}(\beta)$. Consequently, the transmit pulse shapes need to be determined before the proposed power estimation procedures are conducted. We introduce an ANN classifier based roll-off factor estimation scheme which shows

the advantage that it does not require an exact knowledge of other channel parameters, e.g., the CFOs.

Despite the roll-off factors are generally parameters in a continuous valued domain, we adopt an approach for estimation of the roll-off factors that is based on classification by an ANN, here. Not only is the concept of conducting estimation via classification known in the literature on machine learning [22]. We could verify in our previous study on roll-off factor estimation for PCMA signals [23], that a similar ANN based classification approach outperforms a corresponding scheme that employs a regression ANN of equivalent size. Hence, we do not investigate ANNs with regression output, here.

In order to construct a blind roll-off factor estimator for PCMA signals, we formulate the estimation problem as a supervised learning based classification task. To that end, we assume that the possible roll-off factor values that may occur in the respective PCMA satellite system can be expected to lie within a range $[\rho_{\min}, \rho_{\max}]$ that is known at the receiver and is in line with the respective system specifications. Even though in general the roll-off factors may take any value from this range, a classifier may choose an estimate, which then is inherently only an approximation, from a limited number of values. For this, we discretize this expected range of roll-off factor values $[\rho_{\min}, \rho_{\max}]$ for each carrier into a finite discrete set of V roll-off factor values $\{\rho_1, \ldots, \rho_V\}$ with $\rho_\nu = \rho_{\min} + (\rho_{\max} - \rho_{\min})/V \cdot (\nu - 1/2)$, $\nu = 1, \ldots, V$, such that each value lies at the center of one of N equally sized intervals that cover the expected range. Extending this idea to the PCMA signal here, we discretize the space of possible combinations of the two roll-off factors $[\rho_{\min}, \rho_{\max}]^2$ analogously, such that V^2 possible combinations $(\tilde{\rho}_1, \tilde{\rho}_2)_\mu$, $\mu = 1, \ldots, V^2$ are considered in the constructed classification problem with $C = V^2$ classes.

We use an estimate of the time-averaged power spectral density of the received PCMA signal as input to the ANN classifier in our approach. The PSD_0 is a favorable data representation because it contains spectral features that are relevant to the inference of the roll-off factors but is invariant to the symbol timing and carrier phase offsets. Since it is a second-order statistic, it is not affected by the large estimation variances of higher-order statistics. The estimation variance can be further reduced by averaging a large number of windowed sub-segments of a long segment of the signal. An accurate representation of the PSD_0 by its estimate is especially beneficial for a blind receiver. At the same time, the input dimension L is kept constant for varying lengths of the signal segment used for the estimation of the PSD_0.

Given the assumption that the data symbols $a_{i,k}$ are independent with respect to i, and k, the PSD_0 of the received signal is given by (cf. e.g. [24, Ch. 4])

$$\bar{\Phi}_{rr}(f) = \frac{1}{T}\sum_{i=1}^{2} E_{\mathrm{S},i}\left|G_{i,1}(f - f_i)\right|^2 + \Phi_{ww}(f), \qquad (34)$$

where $\Phi_{ww}(f)$ is the power spectral density of the noise $w(t)$, which is primarily determined by N_0 and the input filter transfer function. Averaging M periodograms of distinct frames of L consecutive values of $r[n]$ yields an asymptotically unbiased estimate of the PSD_0 by [25]

$$\hat{\bar{\Phi}}_{rr}(f) = \frac{T_\mathrm{s}}{ML}\sum_{m=0}^{M-1}\left|\sum_{n=n_{0,m}}^{n_{0,m}+L-1} r[n]e^{-\mathrm{j}2\pi f n T_\mathrm{s}}\right|^2, \qquad (35)$$

where $n_{0,m} = n_0 + mL$ and the choice of the anchor sample index n_0 is arbitrary and does not restrict generality if a PCMA signal with infinite support is assumed. For our experiments, we choose to evaluate (35) for frequencies $f = 0, \ldots, (L-1)/(LT_\mathrm{s})$, which corresponds to the standard grid of the discrete Fourier transform domain. Thus, each PSD_0 estimate is represented by L frequency values.

The goal of the design of the ANN is to map the estimated PSD_0 input to a hypothesis of the pair of roll-off factors of the two carriers of the received signal. The implementation of such mapping is accomplished by a supervised learning process using synthetic training data which is generated by standard simulation software according to the system model (1), (2). The collection of data samples which are labeled PSD_0 estimates form the training data set $D = \{(\hat{\bar{\Phi}}_{rr,\delta}(f), y_\delta), \delta = 1, \ldots, |D|\}$ of size $|D|$, where $y_\delta \in \{1, \ldots, C\}$ are the class labels of the δ-th training example $\hat{\bar{\Phi}}_{rr,\delta}(f)$. Here, for PCMA signals, each class number $y \in \{1, \ldots, C\}$ stands for a certain roll-off factor combination $(\rho_1, \rho_2)_y \in \{\rho_1, \ldots, \rho_V\}^2$. For training the ANN, the roll-off factors of the generated signals from which the input examples are obtained by the estimation procedure (35) are chosen from the discrete set $\{\rho_1, \ldots, \rho_V\}^2$.

It should be emphasized here, that the ANN is provided only with the estimate of PSD_0. No further side information like, e.g., on the CFOs is available at the input of the ANN. Further, apart from adjusting the sampling rate to an integer multiple of the symbol rate and adjusting the power levels such that they lie within a certain range, no synchronization is performed prior to the PSD_0 estimation. Consequently, neither the respective channel nor signal parameters are conveyed to the network implicitly and follow the same assumptions as outlined in Section II. Only the range of parameter values represented by the training is thereby known to the trained ANN. Further details on the particular parameter values used for our numerical evaluations are provided in Section V.

The employed network architecture is based on a conventional convolutional neural network (CNN) architecture, which is generally a subcategory of ANNs. This choice is in line with other related works on the estimation of communication signal parameters by deep learning based classifiers [26]. The details of the layout of the adopted ANN are specified in Table 1. As pointed out above, the network input is the PSD_0 estimate comprised in a real one-dimensional vector of L elements that correspond to L frequencies. We choose $L = 1024$ for a trade-off between processing a detailed representation of the PSD_0 estimate and limiting the network complexity.

First, two convolutional blocks process the input data. The convolutional blocks consist of several layers as follows.

TABLE 1. Architecture layout of the CNN roll-off classifier.

Layer	Output dimension
Input	1×1024
Convolutional layer 1	4×1024
Batch normalization	4×1024
ReLU activation	4×1024
Max-pooling	4×512
Convolutional layer 2	4×512
Batch normalization	4×512
ReLU activation	4×512
Max-pooling	4×256
Fully-connected 1	512
ReLU activation	512
Fully-connected 2	N^2
Softmax	N^2

The first layer is a convolutional layer with four trainable 1D filters of size 64 that are convolved with the respective input and are meant to extract features from the input signal. Before the respective convolution operation, zero-padding is applied to the input such that the second output dimension equals the input dimension. The second layer performs batch normalization in order to regularize and stabilize the learning process. Each data batch is normalized by normalization during training. Third, a rectified linear unit (ReLU) activation function performs non-linear mapping in the ANN. The final step of the convolutional block is max-pooling. Here, the output dimension is reduced by a factor of 2 by downsampling while the most important extracted information shall be retained.

The learned features at the output of the second convolutional block are flattened and processed by two fully-connected layers. The first fully-connected layer comprises 512 neurons and is followed by another ReLU activation layer. The number of neurons of the second fully-connected layer equals the number of classes C. The last layer is a Softmax activation function which estimates the occurrence probability p_y of each class $y \in \{1, \ldots, C\}$, given the input $\hat{\bar{\Phi}}_{rr}(f)$. Finally, the estimated roll-off factor combination is inferred from the output of the ANN as the roll-off factor pair $(\rho_1, \rho_2)_y$ that corresponds to the class label index y, for which the output of the Softmax layer is maximized, i.e,

$$\left(\hat{\rho}_1, \hat{\rho}_2\right) = (\rho_1, \rho_2)_{\hat{y}}\,, \quad \hat{y} = \underset{y \in 1,\ldots,C}{\operatorname{argmax}}\, p_y. \tag{36}$$

In this paper, we focus on investigating the processing chain comprising the ANN-based roll-off factor estimation that acts as key enabling step for the subsequent power estimation by the schemes described in Section III. The design of the ANN, including the choice of the number of the convolutional blocks and the number and size of filters therein, as well as the number of neurons in the fully-connected layer are based on our experience from experimenting across several data sets. Here, we have focused on achieving a satisfactory and robust classification performance while maintaining a relatively low computational complexity, which is especially advantageous during the inference phase. Further, we emphasize that no exhaustive tuning of the hyperparameters has been conducted, and we do not claim their respective selection to be optimal. The performance of the ANN based scheme may be further improved by a rigorous tuning for specific system models. Strictly optimizing the ANN design towards maximal classification accuracy or minimal estimation error is beyond the scope of this paper. Yet, we show in Section V on the experimental system evaluation that the attained performance is sufficiently good such that the performance of the subsequent power estimation deteriorates only slightly, compared to ideal knowledge of the roll-off factors.

In practice, the training of the ANN may rely on a training data set of limited size. Such limitation can lead to overfitting of the trained model. This behavior can be addressed by employing regularization methods for the ANN like Dropout or L2 regularization.

V. NUMERICAL PERFORMANCE EVALUATION

In this section, the estimation accuracy of the power and roll-off factor estimation schemes presented above is evaluated. For this purpose, we have generated synthetic discrete-time representations of the PCMA signals according to the model (1), (2). We normalize the sampling period to $T_S = 1$ with a symbol period of $T = 10$, i.e., 10 samples per symbol are taken. The modulation schemes used for both carriers are specified for each of the subsequent experiments. The upper and lower limits of the interval within which the roll-off factors ρ_i of the respective root-raised-cosine transmit pulses shall be assumed to lie are $\rho_{\min} = 0.2$ and $\rho_{\max} = 0.5$. These choices are in line with the specification of roll-off factors in modern commercial standards [27]. Concerning the channel parameters, the carrier phases and symbol timing offsets of the two carriers are chosen randomly from the respective domains following a uniform distribution, i.e. $\phi_i \sim U[0, 2\pi)$ and $\tau_i \sim U(-T/2, T/2]$, for $i = 1, 2$, respectively. The frequency offsets f_i of both carriers are chosen subject to a uniform distribution around zero with a magnitude of not more than five percent of the symbol rate, i.e., $f_i \sim U[-f_{\max}, f_{\max}]$ with $f_{\max} = 0.05/T$. The filter at the receiver input is designed to approximate an ideal lowpass with one-sided bandwidth $B = (1 + \rho_{\max})/(2T) + f_{\max}$. The energy per symbol of the respective carriers is uniformly distributed with deviation of ± 1 dB around unity, i.e., $10 \log_{10}(E_{S,i}) \sim [-1\,\text{dB}, 1\,\text{dB}]$. The SNR used for illustrating the following results is defined by $\text{SNR} = (E_{S,1} + E_{S,2})/(T \cdot 2BN_0)$. The PSD_0 estimates are obtained from the received signals according to (35).

A. EVALUATION OF THE ANN BASED ROLL-OFF-FACTOR ESTIMATOR

For training the ANN-based estimator for the roll-off-factors of the two carriers, we have generated data sets that contain PSD_0 estimates of simulated received signals with parameters as described in the beginning of this section. In the training process, a Stochastic Gradient Decent with momentum algorithm is employed for the minimization of the categorical cross-entropy loss function as metric for the classification performance, running over 100 epochs with a learning rate of

0.0045 and a batch size of 64. For training the classification ANNs, the roll-off factors have been chosen from a discrete grid on the interval $[\rho_{\min}, \rho_{\max}]$ as described in Section IV, i.e., $\{\rho_{\min}+(\rho_{\max}-\rho_{\min})/V\cdot(\nu-1/2), \nu \in \{1,\dots,V\}\}$. The respective sample of a training data set features the roll-off factor combination $(\rho_1, \rho_2)_\mu$, where μ thus represents the class that the data sample is associated with. In the training data set, each sample includes a PSD_0 estimate that serves as ANN input and the corresponding label, that is used for calculating the loss during training. Regardless of the number of classes, data sets for training contain $|D| = 27 \cdot 10^4$ signal examples. Because the data symbols of the modulation constellation have unit average power, the actual used modulation has no effect on the PSD_0. Accordingly, we could verify that the particular symbol constellation selected from the set of considered modulation schemes has negligible influence on the roll-off factor estimation by the ANN, which uses an estimate of the PSD_0 as input. Hence, QPSK modulation has been chosen for the generation of all training set samples. The SNR in dB-scale of the training data set is uniformly distributed according to SNR $\sim$ [0 dB, 25 dB].

Meanwhile, we test the trained ANN-based roll-off estimators on signal examples that were generated with roll-off factors which are not picked from the discrete training grid but are continuously uniformly distributed on $[\rho_{\min}, \rho_{\max}]$, i.e., they do not exactly match the roll-off factors of the training examples. However, the classification ANN is supposed to infer the roll-off factors of the test input signal according to the discrete values it is trained on. While the roll-off factors of the test data sets are random, the SNR is respectively constant and each distinct set contains 10^5 examples per SNR value. The employed performance metric for our experiments is the empirical mean-square error (MSE), which is adequate because the roll-off factors of the test data sets are continuously distributed. The MSE is calculated across the estimates for the roll-off factors of both carriers, i.e., the estimates for both carriers are treated as independent from each other and both respective errors contribute to the total MSE.

For the performance evaluation of the roll-off factor estimation scheme we average the performance of the ANNs obtained for three different training trials for the same test data set in order to mitigate the effect of random initialization of the training on the analysis. In contrast, the performance evaluation of the power estimation schemes in the next subsection is based on the roll-off factor estimates of the ANN that achieved the best test performance after training.

In Fig. 3, the MSE of the estimator (36) based on the ANN architecture presented in Section IV (summarized in Table 1) is given for classifiers with different number of classes. Here, the range of possible roll-off factors was discretized into $V = 3, 4, 5, 6$ values such that the respective classifiers distinguish between $C = V^2 = 9, 16, 25, 36$ classes. The number of periodograms for estimating the PSD_0 for training and testing is $M = 100$ for all cases. Regardless of the employed number of classes C, the MSE is decreasing for increasing SNR, as expected. For low SNR, the MSE is similar for all C, while for high SNR, the MSE for the respective cases

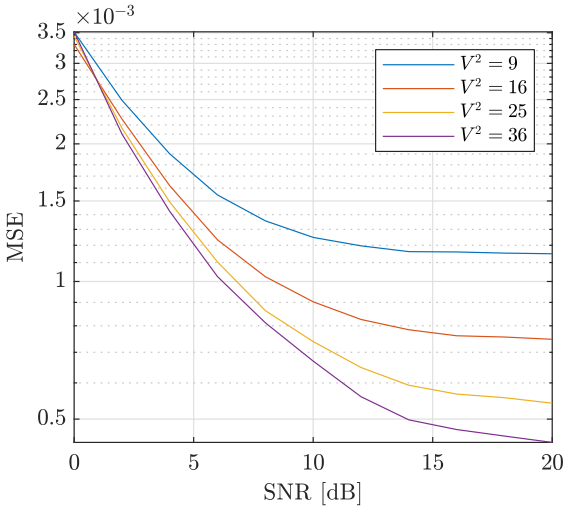

FIGURE 3. MSE of the ANN classifier based roll-off factor estimator for PCMA signals for different numbers of classes representing discrete samples of the roll-off factor domain.

reaches an error floor with an individual level of MSE. Based on the results in Fig. 3 we observe that increasing C yields a decreased MSE throughout almost the entire evaluated SNR range. Yet, the gain from increasing the number of discrete considered values per roll-off factor V by one is getting smaller for higher number of classes, e.g., the gain from increasing $C = V^2$ from 16 to 25 is larger than the gain from increasing $C = V^2$ from 25 to 36. A higher resolution of discrete roll-off factor values naturally allows for an increased precision of the estimates, as the distance from the output estimate to a value that lies within the domain between two discrete values becomes smaller. Assuming that the closest discrete value to the true value is selected by the classifier based estimator, the minimum obtainable error is thus decreased. However, a saturation effect is observed from Fig. 3. This behavior is an indication for underfitting which may occur due to the incapability of the ANN to approximate the inference function that maps the PSD_0 at the input to estimator outputs that represent values close to each other. The effect becomes especially apparent in the case of a large number of classes. Unless the complexity of the ANN or the training set size is increased, the gain from increasing the number of classes is not promising [23]. By increasing the network complexity, altering its architecture and optimizing the hyperparameters of the learning process, the MSE may be further decreased. In this paper, the goal of introducing the ANN-based roll-off factor estimator is not to obtain arbitrarily low estimation variance, but to enable the usage of the subsequent carrier power estimators. We show that this goal is sufficiently attained in the next subsection, where an ANN-based estimator of the presented type is used to provide the respective roll-off factor estimates for the statistics-based power estimators.

B. EVALUATION OF THE POWER ESTIMATORS

In this subsection, we evaluate the power estimation approaches introduced in Section III. For this purpose, we parameterize the length of the signal segment that is used

for the estimation of the statistical quantities employed in the different power estimators by the number of contained symbol intervals N_S. Thus, matching our definition of the cyclic moment estimator (16), which is used for obtaining all required statistics, the processed signal segments contain $2N+1$ signal samples and N is chosen such that N_S symbol intervals are contained in this segment, i.e., $N = \lceil (N_S T/T_S - 1)/2 \rceil$, where an integer oversampling factor T/T_s is assumed. The PSD_0 estimates contained in the training data sets for the learning process as described in the previous subsection were obtained by using a fixed number of periodograms M which translates to a respective signal segment length. In contrast, the PSD_0 estimates used for the inference phase of the ANN in the current section are obtained exploiting the whole available signal segment, such that $M = \lfloor (2N+1)/L \rfloor$ periodograms are obtained from distinct windowed sub-segments. The specific ANN employed in the roll-off factor estimator that is used to provide the respective values to the subsequent estimators for the powers or energies per symbol, respectively, is trained with PSD_0 estimates calculated using $M = 100$ frames of length $L = 1024$ and $C = 25$ classes for inference of the roll-off factor combination.

Throughout this subsection, we abbreviate the symbol energy estimator (19) of Section III-B1 as "V1", the estimator (29) or (25), (26), respectively, of Section III-B2 as "V2", and the mixed approach of (31) of Section III-B3 by "Mix". Additionally, we evaluate the performance of the approach for estimation of the energy per symbol that is conducted implicitly in the scheme in [8]. An explicit expression is derived to

$$\hat{E}_{S,i} = \underset{\tilde{E}_{S,i}}{\operatorname{argmin}} \sum_{p \in P} \left| \hat{C}_{r,(p,0)}(pf_i) - \tilde{E}_{S,i} C_{s_i,(p,0)}(0) \right|^{p/2}, \quad (37)$$

where $P = \{2, 4, 6, 8\}$ is the set of employed cumulant orders. This scheme is used as a benchmark scheme for the energy per symbol estimators introduced in this paper and is labeled by "Wang" in Fig. 4 and Fig. 5.

The metric for evaluating the accuracy of estimating the energy per symbol of the respective carriers is again the empirical MSE, averaged over both carriers.

In Fig. 4, we compare the MSE of estimators V1, V2 and Mix versus SNR for different modulation schemes. Estimators V1 and V2 are evaluated for the case where both carriers are QPSK-modulated (referred to as QxQ in the figure legend), the case of 8PSK modulation for both carriers (denoted as 8×8), and the case in which one carrier is of QPSK modulation and the other carrier is of 8PSK modulation (denoted as Qx8 in the figure legend). Since the Mix estimator is designed for the case where only one of the two carriers is 8PSK-modulated, we showcase the estimation performance of the Mix approach for the case in which one carrier is 8PSK-modulated and the other one is QPSK-modulated, only. The utilized signal segment contains $N_S = 10^5$ symbol intervals for all schemes and modulation combinations, here.

It can be seen that the MSE for all schemes and modulation combinations is decreasing over SNR for values up to approximately 22 dB until an error floor is reached. For the estimators V1 and V2, the MSE for the 8×8 modulation combination case is highest, followed by the mixture case Qx8, and the MSE for the case of QxQ modulation combination is lowest, of the evaluated ones. Further, the MSE of the estimator V1 for the QxQ case is almost one order of magnitude below the MSE of the V2 estimator evaluated for the same case. However, for the cases, in which one or both carriers are 8PSK-modulated, employing the estimator V2 provides a significant performance gain over estimator V1. We interpret this gain as being achieved through avoiding the estimation of cyclostationary properties of order $p = 8$, and employing the sixth-order (6,3) cumulant as statistic with highest necessary order, instead. The best possible performance for the Qx8 case is obtained by the Mix estimator, that exploits statistics of orders not higher than $p = 4$, i.e., $C_{r,(4,2)}(0)$, here. These observations support the notion that estimates of statistics of high orders are error-prone for limited SNR and signal segment length, and corresponding parameter estimators are less accurate. The MSE of the "Wang" reference scheme is identical to that of the V1 scheme in the cases of Qx8 and 8×8 modulation and slightly above the MSE of the V1 estimator in the QxQ case for low-to-medium SNR. Thus, the proposed V1 scheme outperforms the "Wang" reference scheme in the QxQ case. At the same time, the proposed V2 scheme outperforms the "Wang" reference scheme for all cases that include 8PSK modulation.

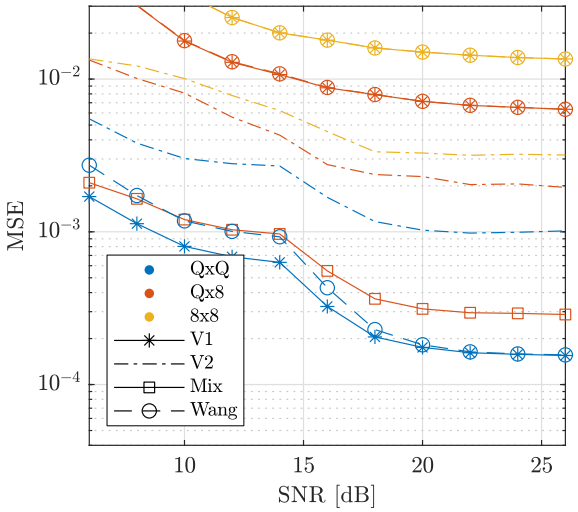

FIGURE 4. MSE of the V1, V2, and Mix energy per symbol estimation approaches for PCMA signals versus SNR for different combinations of carrier modulation schemes and a signal segment length of $N_S = 10^5$ symbol intervals.

In Fig. 5, the same combinations of estimation approaches and modulation schemes as before are evaluated for a fixed SNR of 20 dB, and different lengths of the signal segment. For all investigated cases, the MSE decreases for increasing N_S. The ordering of achieved MSE of different estimation schemes in each case is identical to the order in the previous experiment throughout the entire range of the segment length N_S. It can though be observed for estimator V2 that for increasing N_S in a high N_S regime no further MSE improvement can be obtained.

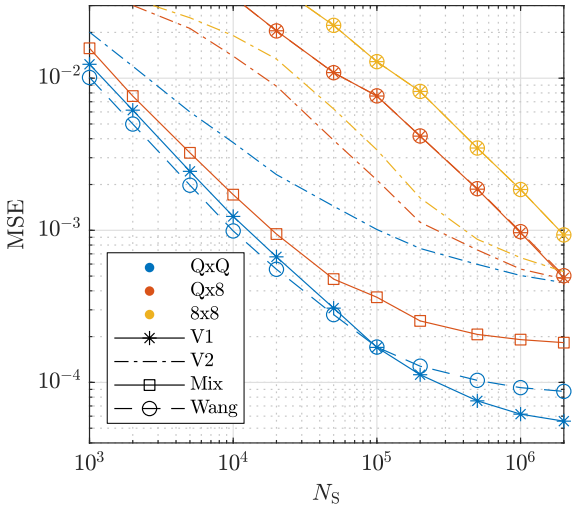

FIGURE 5. MSE of the V1, V2, and Mix energy per symbol estimation approaches for PCMA signals versus the length of the signal segment specified by the number of contained symbol intervals N_S for different combinations of carrier modulation schemes and an SNR of 20 dB.

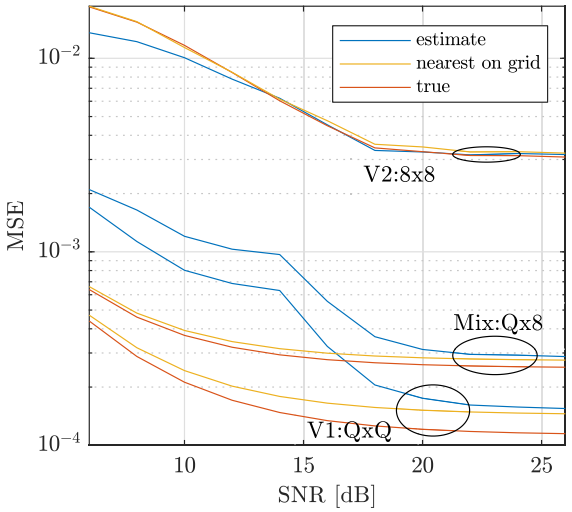

FIGURE 6. MSE of the energy per symbol estimators versus SNR for PCMA signals for true and estimated roll-off factors. The estimates are obtained from signal segments containing $N_S = 10^5$ symbols.

Consequently, for N_S at the upper edge of the evaluated range, the performance of the estimators V1 and V2 and the "Wang" reference scheme is similar if at least one of the modulations is 8PSK. Again, for the QxQ-case, the performance of the V1 estimator is unmatched by the V2 estimator and surpasses the performance of the "Wang" reference scheme for large N_S. For the Qx8 case, the Mix approach yields the lowest MSE of the evaluated estimation schemes. From the results of Fig. 4 and Fig. 5 we can conclude that in the case of 8PSK modulation of both carriers, the estimation accuracy of approach V1 and the "Wang" reference scheme can be improved by approach V2 for medium sized segment lengths.

Results of an experiment that investigates the impact of the errors of the ANN-based roll-off factor estimator are depicted in Fig. 6. Here, the MSE of the energy per symbol estimators is considered for the case in which the roll-off factor estimate of the ANN is used in the subsequent processing steps of the energy per symbol estimators, and for two genie-aided cases. The results for the case in which the actual estimate of the ANN is used are illustrated by the blue lines in Fig. 6, and the corresponding legend label is "estimate". In the first genie-aided case, the true roll-off factors are provided to the power estimators. It is depicted in Fig. 6 by the red lines and labeled with "true" in the figure legend. In the second genie-aided case, that roll-off factor combination on the classifier grid is provided to the subsequent power estimators, which is closest to the true combination. The results for this case are shown by the yellow lines in Fig. 6 and labeled by "nearest on grid" in its legend. All estimates are obtained from signal segments containing $N_S = 10^5$ symbols. Since we could observe that for the case of QxQ modulation the V1 estimator provides the lowest MSE, and for the Qx8-case the Mix estimator and for the 8×8 case the V2 estimator have the best performance, only the results for those estimators are shown for the respective modulations. From the results for the QxQ and Qx8 cases, it can be seen that for low-to-medium SNR, the performance of the power estimators deteriorates due to the influence of the errors of the roll-off factor estimator, while for medium-to-high SNR the performance when using the actual estimates is close to that for genie-based knowledge of the roll-off factors. Hence, we can conclude that our goal of designing an estimator that provides sufficiently accurate roll-off factor estimates in order to facilitate the subsequent power estimation is achieved by the ANN-based estimator of Section IV. Further, by inspecting the results for the case in which the closest possible roll-off factor combination on the grid corresponding to the discrete roll-off factors that are represented by the classifier is chosen, we observe that the finite resolution of the classifier has only limited influence on the accuracy of the power estimation. The case of the genie-aided choice of the roll-off factor combination on the grid which is closest to the true combination is a performance upper bound for the case where the actual ANN-based estimate is used, and it can be seen that this bound is nearly attained by the estimator. We conclude that the design and training of the ANN is appropriate with respect to the desired power estimation. In the 8×8 case of 8PSK modulation, where only a rather high MSE can be achieved, even if the true roll-off factors are provided by a genie-based scheme, the performance is almost unaffected. Thus, we see that the influence of imperfect roll-off factor estimates is limited.

The performance of the noise power estimation according to (33), which exploits the previously obtained energy per symbol estimates, is shown in Fig. 7. In particular, the cases of QPSK modulation (QxQ) and 8PSK modulation (8×8) of both carriers, respectively, are considered. Here, the normalized MSE (NMSE), i.e., mean-square of the error of the noise power estimation divided by the actual squared noise power, is shown versus SNR. For both cases, we compare the NMSE of the noise power estimation based on the energy per symbol estimates of the V1 estimator, the V2 estimator and the ground-truth values of the energy per symbol, respectively. For increasing SNR, the noise power decreases compared to the

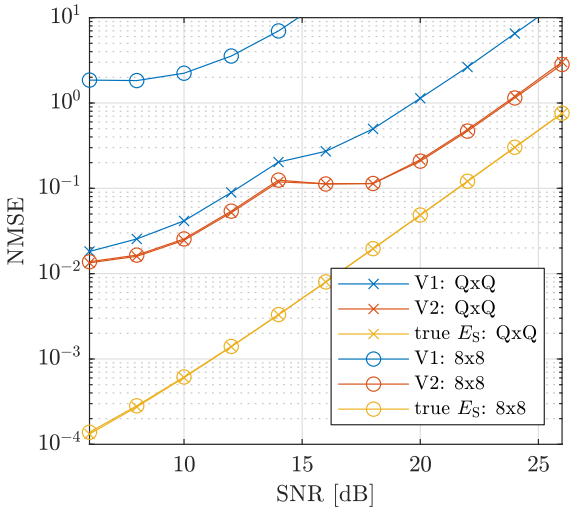

FIGURE 7. Normalized MSE (NMSE) of the noise power estimation for PCMA signals versus SNR using the energy per symbol estimates of the V1 and V2 estimator with $N_S = 10^5$ and the true energies per symbol for different carrier modulation combinations.

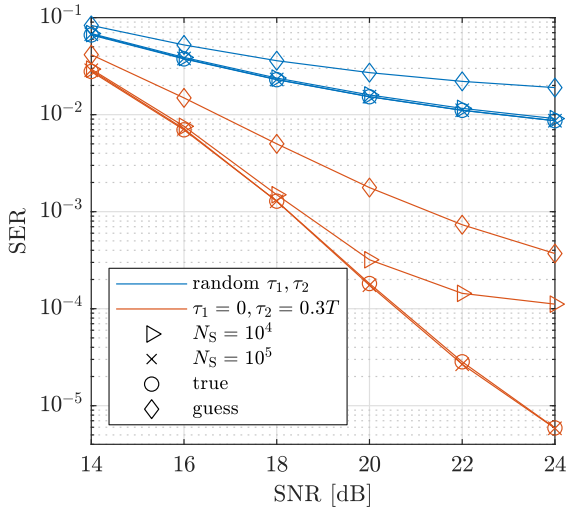

FIGURE 8. SER of the approximate joint MLSE for PCMA signals with QPSK modulation versus SNR for the estimation of the roll-off factors and energies per symbol by the ANN and V1 estimator, respectively, using the corresponding true values and using values chosen as the centers of the range of possible values.

total signal power. Consequently, it can observed in Fig. 7 that the NMSE increases with increasing SNR for all cases, even if the true values for $E_{S,i}$, $i = 1, 2$ are used for the estimation of the noise power. While there is a significant gap between the noise power NMSE of QxQ and 8×8 modulation in the case of estimating the energies per symbol by the estimator V1, the noise power estimation based on the estimates of the energy per symbol of the V2 estimator shows almost identical NMSE for both considered modulations. Interestingly, for both modulations, utilizing the energy per symbol estimates of V2 results in an improved NMSE compared to adopting the estimates of V1. This seems counterintuitive for the case of QxQ modulation, since for this case it can be concluded from Fig. 4 that the MSE of the individual energy per symbol estimate by V1 is lower than that of the V2 estimate. However, a numerical evaluation shows that the sum of the estimates for the energy per symbol by the approach V2 yields a lower MSE w.r.t. the sum of the true energies per symbol, compared to the sum of the energy per symbol estimates obtained using V1. As a direct consequence, the NMSE of the noise power estimation is lower when the energy per symbol estimates of V2 are used, compared to V1. For both modulations, the NMSE that is achieved when the true energy per symbol values are used for noise power estimation cannot be attained by using values provided by any of the estimators.

C. EVALUATION OF SYMBOL DETECTION USING THE PROPOSED ESTIMATORS

Finally, we evaluate the effect of using the proposed estimators on the detection performance of a sequence estimation scheme for PCMA. Our adopted detection scheme is based on the joint maximum-likelihood sequence estimation (MLSE) approach according to [28], which is adapted to the PCMA signal model. Here, simplifications are introduced in order to limit the computational complexity. Thus, we refer to the scheme as approximate joint MLSE. Furthermore, QPSK modulated signals are considered in order to limit the complexity of the detector used in the evaluation. Since we aim at assessing the performance of the roll-off factor and energy per symbol estimators when used in detection, all other channel parameters are assumed to be known to the receiver and selected randomly for each Monte-Carlo trial. The obtained symbol error rate (SER) shown in Fig. 8 is averaged over both carriers. We have observed that the SER is especially affected by the symbol clock phases of both carriers. Thus, additional results are shown for fixed values $\tau_1 = 0$, $\tau_2 = 0.3T$, for which a relatively low SER can be achieved. The roll-off factors are obtained using the same ANN based estimator as in the previous subsection, and the V1 estimator is used for estimating the energies per symbol. We investigate two cases of signal segment length of $N_S = 10^4$ and $N_S = 10^5$, respectively, used by the estimators. The SER is compared to that of the case in which the true values of the roll-off factors and energies per symbol are used in the detector and the case in which no estimation is performed but the center of the respective interval of a parameter is chosen by default. The two latter cases are termed "true" and "guess", respectively, in the figure legend. For random symbol clock offsets, only relatively high SERs of approximately 10^{-2} can be achieved within the considered SNR range by the detection in both cases of using either true or estimated roll-off factors and energies per symbol, because the SER is dominated by simulation runs with $\tau_1 \approx \tau_2$ which is unfavorable for PCMA detection. Only for the "guess" case in which no actual estimation is performed, the SER is even higher. We conclude that for harsh random channels, the estimation accuracy of the proposed estimators is sufficient, even for short-to-medium signal segments containing $N_S = 10^4$ symbols. For the more advantageous channel with symbol clock offsets $\tau_1 = 0$, $\tau_2 = 0.3T$, the SER that can be achieved by the detector that uses the ground-truth parameter values is approximately three

to four orders of magnitude lower than that in the previous case. On the other hand, if no estimation is carried out and the respective parameter values used in the detector are just selected as the centers of their domains (label ''guess''), the SER is increased by about two orders of magnitude. Hence, we conclude that providing accurate estimates for the roll-off factors and energies per symbol is crucial for obtaining a low SER in relatively good channel conditions. When a signal segment of $N_S = 10^4$ symbols is used for estimation, the attained SER is more than one order of magnitude higher than in the case of the true parameters and the respective curve in Fig. 8 flattens out to an error floor. This error floor is very likely due to the distortion that is introduced by the inaccurate modeling of the received signal with imperfect parameter estimates in the detector. On the contrary, when the signal segment length is increased to $N_S = 10^5$, the SER can be reduced to become almost identical to that of the case where the true parameters are used in the detector. Thus, for medium signal segment lengths, the estimates for the roll-off factors and energies per symbol are sufficiently accurate to ensure no deterioration of the detector performance.

VI. CONCLUSION

In this paper, we have presented estimation schemes for the power, or equivalently the energy per symbol, of the carriers of a PCMA signal, based on estimation of cyclostationary properties of the received signal. Simulation results show that the carrier powers can be estimated with good precision by the presented approaches. For higher-order modulation, e.g. 8PSK, the V1 estimator relies on the statistics of high order, i.e., in this case, the eighth-order cyclic cumulant $C_{r,(8,0)}(8f_i)$ and suffers from a high estimation variance for limited-size signal segments. Therefore, we have introduced alternative estimation schemes that only require statistics of lower orders. Hence, in the case in which both carriers are 8PSK-modulated, the V2 power estimator that employs the sixth- and fourth-order cyclic cumulants $C_{r,(6,3)}(0)$ and $C_{r,(4,2)}(0)$ can achieve lower MSE for medium-sized signal segments. In this case, it may be attempted in future investigations to identify other lower-order statistics with which an MSE comparable to that for QPSK modulation can be achieved. If only one carrier is 8PSK-modulated, the best performance is achieved by the Mix estimator, that estimates the power of the other carrier first and then uses the fourth-order cyclic cumulant $C_{r,(4,2)}(0)$ to infer the power of the carrier with 8PSK modulation.

Interestingly, the noise power estimation is more robust if the V2 estimator is used for the carrier power estimation, because the sum of the powers is more accurately estimated by this scheme for all considered modulations.

Applying the presented estimation schemes for the carrier power is facilitated through a preceding roll-off factor estimation. For this purpose, we have introduced a simple ANN-based estimator to infer the combination of the roll-off factors of the two carriers, based on an estimate of the PSD_0 of the received signal. Designing this estimator as a classifier proved to be effective for different resolutions of the discrete set representing a limited range of possible roll-off factors. Furthermore, our experiments showed that the accuracy of the power estimators is only slightly affected by the roll-off factor estimation errors for sufficiently high SNR.

We could also confirm that a subsequent sequence estimation scheme employing parameters delivered by the proposed estimators achieves SERs similar to those for the case of perfect knowledge of the parameters.

ACKNOWLEDGMENT

An earlier version of this paper was presented at the 2025 IEEE Consumer Communications & Networking Conference, Las Vegas, NV, USA.

REFERENCES

[1] M. Dankberg, ''Paired carrier multiple access (PCMA) for satellite communications,'' in *Proc. 17th AIAA Int. Commun. Satell. Syst. Conf. Exhibit*, Yokohama, Japan, Feb. 1998, p. 1398.

[2] C. Agne, Maj. B. Cornell, M. Dale, R. Kearns, and F. Lee, ''Shared-spectrum bandwidth efficient satellite communications,'' in *Proc. Mil. Commun. Conf. (MILCOM)*, San Jose, CA, USA, Oct. 2010, pp. 341–346.

[3] G. D. Collins and J. Treichler, ''Practical insights on full-duplex personal wireless communications gained from operational experience in the satellite environment,'' in *Proc. IEEE Signal Process. Signal Process. Educ. Workshop (SP/SPE)*, Salt Lake City, UT, USA, Aug. 2015, pp. 136–141.

[4] A. Feder, M. Hirschbeck, and W. Gerstacker, ''Blind estimation of the carrier powers and SNRs in PCMA satellite signals by cyclic statistics,'' in *Proc. IEEE Mil. Commun. Conf. (MILCOM)*, Rockville, MD, USA, Nov. 2022, pp. 913–919.

[5] C. Colavolpe, G. Ferrari, and R. Raheli, ''Reduced-state BCJR-type algorithms,'' *IEEE J. Sel. Areas Commun.*, vol. 19, no. 5, pp. 848–859, May 2001.

[6] X.-B. Liu, Y. L. Guan, S. N. Koh, Z. Liu, and P. Wang, ''Single-channel blind separation of co-frequency PSK signals with unknown carrier frequency offsets,'' in *Proc. IEEE Mil. Commun. Conf. (MILCOM)*, Baltimore, MD, USA, Oct. 2017, pp. 641–646.

[7] G. Wang, S. K. Ting, S. G. Razul, and C. M. S. See, ''Single channel blind separation of non-orthogonal cochannel signals with higher order modulation,'' in *Proc. IEEE 23rd Int. Conf. Digit. Signal Process. (DSP)*, Shanghai, China, Nov. 2018, pp. 1–5.

[8] G. Wang, H. Guo, G. Bi, S. K. Ting, and S. Razul, ''Automatic modulation classification of cochannel communication signals based on cumulant,'' in *Proc. IEEE 23rd Int. Conf. Digit. Signal Process. (DSP)*, Shanghai, China, Nov. 2018, pp. 1–5.

[9] M. Liu, S. Yu, Y. Chen, and S. Chen, ''Blind parameter estimation for co-channel digital communication signals,'' *Wireless Netw.*, vol. 30, no. 6, pp. 5589–5599, Mar. 2023.

[10] R. Matzner and F. Englberger, ''An SNR estimation algorithm using fourth-order moments,'' in *Proc. IEEE Int. Symp. Inf. Theory*, Jun. 1994, p. 119.

[11] D. R. Pauluzzi and N. C. Beaulieu, ''A comparison of SNR estimation techniques for the AWGN channel,'' *IEEE Trans. Commun.*, vol. 48, no. 10, pp. 1681–1691, Oct. 2000.

[12] A. Feder, W. Wicke, M. Hirschbeck, and W. Gerstacker, ''Blind symbol rate and frequency offset estimation for PCMA signals via cyclic correlations,'' in *Proc. IEEE GLOBECOM*, Taipei, Taiwan, Dec. 2020, pp. 1–12.

[13] A. Feder, W. Gerstacker, and M. Hirschbeck, ''Blind symbol timing and carrier phase estimation for PCMA satellite signals via cyclic statistics,'' in *Proc. IEEE Global Commun. Conf. (GLOBECOM)*, Madrid, Spain, Dec. 2021, pp. 01–07.

[14] H. Xu, Y. Zhou, and Z. Huang, ''Blind roll-off factor and symbol rate estimation using IFFT and least squares estimator,'' in *Proc. Int. Conf. Wireless Commun., Netw. Mobile Comput.*, Sep. 2007, pp. 1052–1055.

[15] M. Ionescu, M. Sato, and B. Thomsen, ''Cyclostationarity-based joint monitoring of symbol-rate, frequency offset, CD and OSNR for Nyquist WDM superchannels,'' *Opt. Exp.*, vol. 23, no. 20, p. 25762, 2015.

[16] N. Thomas, J.-Y. Tourneret, and E. Bourret, ''Blind roll-off estimation for digital transmissions,'' *Signal Process.*, vol. 135, pp. 87–95, Jun. 2017.

[17] J. Sun, G. Wang, Z. Lin, S. G. Razul, and X. Lai, "Automatic modulation classification of cochannel signals using deep learning," in *Proc. IEEE 23rd Int. Conf. Digit. Signal Process. (DSP)*, Nov. 2018, pp. 1–5.
[18] C. M. Spooner, "Classification of co-channel communication signals using cyclic cumulants," in *Proc. 29th Conf. Rec. Asilomar Conf. Signals, Syst. Comput.*, vol. 1, Pacifc Grove, CA, USA, Oct. 1995, pp. 531–536.
[19] D. R. Brillinger, *Time Series*. Philadelphia, PA, USA: Society for Industrial and Applied Mathematics, 2001.
[20] A. Napolitano, *Cyclostationary Processes and Time Series: Theory, Applications, and Generalizations*. New York, NY, USA: Elsevier, 2019.
[21] A. V. Dandawate and G. B. Giannakis, "Asymptotic theory of mixed time averages and kth-order cyclic-moment and cumulant statistics," *IEEE Trans. Inf. Theory*, vol. 41, no. 1, pp. 216–232, Jan. 1995.
[22] L. Torgo and J. Gama, "Regression using classification algorithms," *Intell. Data Anal.*, vol. 1, no. 4, pp. 275–292, Oct. 1997.
[23] A. Feder, A. Vagollari, R. Fischer, M. Hirschbeck, and W. Gerstacker, "Blind roll-off factor estimation for paired carrier multiple access satellite signals," in *Proc. IEEE CCNC*, Las Vegas, NV, USA, Jan. 2025, pp. 1–14.
[24] J. Proakis, *Digital Communications*. New York, NY, USA: McGraw-Hill, 2001.
[25] P. Stoica and R. Moses, *Spectral Analysis of Signals*. Upper Saddle River, NJ, USA: Prentice-Hall, 2005.
[26] R. M. Dreifuerst, R. W. Heath, M. N. Kulkarni, and J. Charlie, "Deep learning-based carrier frequency offset estimation with one-bit ADCs," in *Proc. IEEE 21st Int. Workshop Signal Process. Adv. Wireless Commun. (SPAWC)*, May 2020, pp. 1–5.
[27] *Broadcasting (DVB); Second Generation Framing Structure, Channel Coding and Modulation Systems for Broadcasting, Interactive Services, News Gathering and Other Broadband Satellite Applications; Part 2: DVB-S2 Extensions (DVB-S2X)*, Standard ETSI EN 302 307-2, Eur. Telecommun. Standards Inst., Jul. 2021.
[28] K. Giridhar, J. J. Shynk, A. Mathur, S. Chari, and R. P. Gooch, "Nonlinear techniques for the joint estimation of cochannel signals," *IEEE Trans. Commun.*, vol. 45, no. 4, pp. 473–484, Apr. 1997.

ANDREAS FEDER (Graduate Student Member, IEEE) received the B.Sc. and M.Sc. degrees in electrical engineering from Friedrich-Alexander-Universität Erlangen-Nürnberg (FAU), Erlangen, Germany, in 2016 and 2019, respectively, where he is currently pursuing the Dr.-Ing. degree with the Institute for Digital Communications. His research interests include communications, with a focus on blind receiver design, synchronization, and parameter estimation.

ADELA VAGOLLARI (Graduate Student Member, IEEE) received the B.Sc. degree in telecommunications engineering from the Polytechnic University of Tirana, Albania, in 2017, and the M.Sc. degree in advanced signal processing and communication engineering (Elite Master's Program within the Elite Network of Bavaria) from Friedrich-Alexander-Universität (FAU) Erlangen-Nürnberg, Germany, in 2020, where she is currently pursuing the Dr.-Ing. degree in electrical engineering with the Institute for Digital Communications. Since 2023, she has been with the Fraunhofer-Institut für Integrierte Schaltungen—IIS, Erlangen, Germany, as a Research Assistant. Her current research interests include applications of machine learning and deep learning in wireless communications, with a focus on RF spectrum analysis and dynamic spectrum sharing.

RODRIGO FISCHER (Graduate Student Member, IEEE) was born in Brasília, Brazil, in 1997. He received the bachelor's degree in electrical engineering from the University of Brasília (UnB), in 2020, and the Master of Science degree from the Friedrich-Alexander-Universität Erlangen-Nürnberg (FAU), Germany, in 2024, after completing the Elite Master's Programme in Advanced Signal Processing and Communications Engineering, part of the Elite Network of Bavaria. He is currently pursuing the Ph.D. degree with the Communications Engineering Laboratory (CEL), Karlsruhe Institute of Technology (KIT), Germany. His research interests include the application of machine learning (ML) techniques to wireless and optical communications, which includes physical layer signal processing and channel coding.

MARTIN HIRSCHBECK was born in Schwabach, Germany, in 1986. He received the Dipl.-Ing. degree in electrical engineering, electronics, and information engineering and the Dr.-Ing. degree from Friedrich-Alexander-Universität (FAU) Erlangen-Nürnberg, Germany, in 2012 and 2016, respectively. He was a Graduate Student with FAU Erlangen-Nürnberg, from 2012 to 2016. In 2016, he joined Innovationszentrum für Telekommunikationstechnik GmbH IZT, Erlangen, Germany, where he is currently a Project Manager and the Head of the GUI/Algorithm Development Team. He has published several articles in the field of information engineering. His research interests include interference mitigation, modulation recognition and analysis, spectrum monitoring, satellite communications, and signal processing in general.

WOLFGANG GERSTACKER (Senior Member, IEEE) received the Dipl.-Ing. degree in electrical engineering and the Dr.-Ing. and Habilitation degrees from Friedrich-Alexander-Universität (FAU) Erlangen-Nürnberg, Erlangen, Germany, in 1991, 1998, and 2004, respectively.

Since 2002, he has been with the Chair of Mobile Communications and Institute for Digital Communications, FAU Erlangen-Nürnberg, where he is currently a Professor. He has conducted various projects with partners from industry. His research interests include digital communications and statistical signal processing, THz communications, 6G and beyond, machine learning for wireless communications, and wireless sensor networks. He was a recipient of several awards, including the Research Award of the German Society for Information Technology (ITG), in 2001, the EEEfCOM Innovation Award, in 2003, the Vodafone Innovation Award, in 2004, the Best Paper Award of EURASIP Signal Processing, in 2006, and the Mobile Satellite & Positioning Track Paper Award of VTC2011-Spring. He has been the Technical Program Co-Chair or the General Co-Chair of several conferences, including BlackSeaCom 2014, VTC2013-Fall, ACMNanoCom 2016, BalkanCom 2019, and WSA 2025. He is an Editor of *Computer Networks* (Elsevier). Currently, he serves as an Area Editor of IEEE TRANSACTIONS ON WIRELESS COMMUNICATIONS (TWC). He was the Chair of the Executive Editorial Committee of IEEE TRANSACTIONS ON WIRELESS COMMUNICATIONS; an Editorial Board Member of IEEE TRANSACTIONS ON WIRELESS COMMUNICATIONS, *Physical Communication* (Elsevier), and *EURASIP Journal on Wireless Communications and Networking*; and a guest editor of several IEEE journals and magazines.